Applied Physics Letters ARTICLE scitation.org/journal/apl

A dual-effect solution for broadband piezoelectric energy harvesting

Cite as: Appl. Phys. Lett. **116**, 063901 (2020); doi: 10.1063/1.5139480
Submitted: 20 November 2019 · Accepted: 28 January 2020 ·
Published Online: 10 February 2020

Bao Zhao,[1,2,3] Jiahua Wang,[4] Junrui Liang,[1,a)] and Wei-Hsin Liao[4]

AFFILIATIONS

[1]School of Information Science and Technology, ShanghaiTech University, 393 Middle Huaxia Road, Pudong, Shanghai 201210, China
[2]Shanghai Institute of Microsystem and Information Technology, Chinese Academy of Sciences, Shanghai 200050, China
[3]University of Chinese Academy of Sciences, Beijing 100049, China
[4]Department of Mechanical and Automation Engineering, The Chinese University of Hong Kong, Shatin, New Territories, Hong Kong, China

[a)]**Electronic mail:** liangjr@shanghaitech.edu.cn

ABSTRACT

Literature has shown that the bandwidth of a piezoelectric energy harvesting (PEH) system can be effectively broadened by introducing nonlinear mechanical dynamics. However, when connected to a practical PEH interface circuit for ac-to-dc conversion, the bandwidth improvement will be impaired because of the electrically induced damping effect. On the other hand, there is another bandwidth broadening solution, in which the resonant frequency is tunable to some extent by carrying out the phase-variable synchronized switch (PVSS) control in practical interface circuits. This Letter reports a synergistic design by combining these two mechanisms toward a dual-effect broadband PEH solution. The theoretical model of this nonlinear and electromechanically coupled system is derived. The experimental result shows that, by introducing the PVSS control to a PEH system, which is composed of a monostable piezoelectric cantilever beam and a practical synchronized switch interface circuit, its bandwidth can be broadened by 18.7%. This dual-effect solution incorporates two bandwidth broadening mechanisms toward practical broadband PEH systems.

In the upcoming Internet of Things (IoT) era, the power supply for distributed devices, such as wireless sensor nodes, has become an intractable issue against the pervasive deployment of IoT devices.[1] Among the exploitable ambient energy sources, the mechanical vibration source is one of the most promising candidates, given its extensive distribution and usability. During the last decade, many research works have focused on vibration energy harvesting, which converts mechanical energy into electricity by using piezoelectric or electromagnetic transducers.[2–6] In particular, piezoelectric transducers have the merits of high power density and simple structure. They are suitable to be used for building compact and integrated energy harvesting systems.

In piezoelectric energy harvesting (PEH), one of the design targets is to broaden the vibration bandwidth. Broadband solutions can be categorized into two sorts: mechanical and electrical ones. One of the most investigated mechanical solutions is to incorporate nonlinearity to energy harvesting systems, given the intrinsic broadband feature of typical nonlinear oscillators.[7] The most studied nonlinear oscillators are monostable or bistable ones.[8,9] The broadband performances with or without external magnets,[10] under different magnet gaps,[11] with multi-stable structures,[12] etc., have been investigated in detail. These studies emphasized mechanical design and bandwidth broadening results; few of them considered the effect of practical PEH interface circuits. However, it was shown that the interface circuit also plays an important role in the system dynamics.[13] This is particularly true when the electromechanical coupling is strong or when a synchronized switch (SS) interface circuit, such as synchronized switch harvesting on inductor (SSHI)[14] or synchronized triple bias-flip interface circuit (S3BF),[15] is used for the ac-to-dc conversion. Most PEH interface circuits induce an additional damping effect in an electrical way.[16] Derived from the synchronized switch interface circuits, recently, some electrical broadband solutions have been proposed by introducing the phase-variable synchronized switch (PVSS) control to the interface circuits, for example, the phase-variable synchronized charge extraction (PV-SCE),[17] PV-SSHI,[18] and PV-S3BF.[19] The PVSS control induces an additional stiffness/mass to a linear system, which

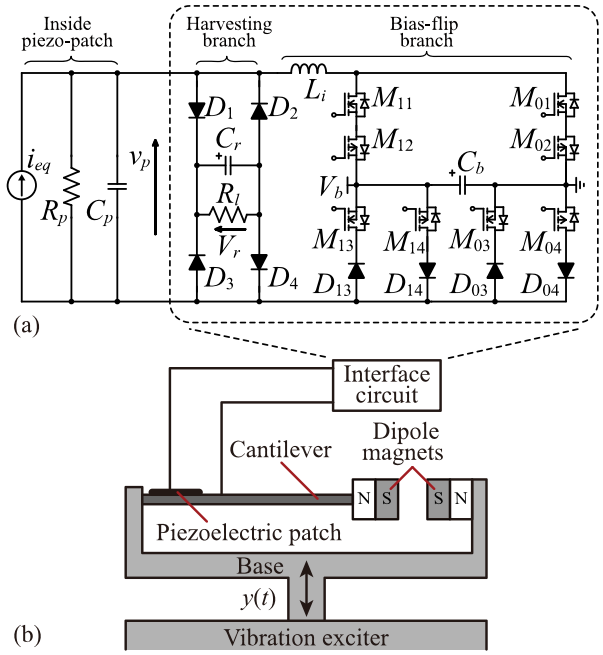

FIG. 1. Dual-effect broadband piezoelectric energy harvester, which is composed of (a) a PVSS interface circuit and (b) a nonlinear structure.

compensates the off-resonant impedance mismatch to some extent. The frequency-tuning capability of PVSS is more significant under strong electromechanical coupling.[20]

In this Letter, we proposed a dual-effect broadband piezoelectric energy harvester (NL-PVSS-PEH) by organically combining the aforementioned two bandwidth-broadening techniques. The collaborative performance of the nonlinear structure and PVSS circuit is studied theoretically and experimentally.

The schematic of an NL-PVSS-PEH system is shown in Fig. 1. The main structure is a cantilever beam with a piezoelectric patch attached near its fixed end. Two repelling magnets are installed at the beam free end and the base frame, respectively, which introduce a nonlinear force to the main structure. In this study, the magnet gap is tuned to realize a monostable nonlinear structure. The output electrodes of the piezoelectric patch are connected to a PVSS circuit for energy harvesting and dynamics tuning. The electrical characteristics of a piezoelectric transducer are summarized by two components: the clamped capacitor C_p and leakage resistor R_p. The PVSS circuit is composed of a full bridge rectifier for energy harvesting and a switch network for carrying out voltage bias-flip actions at displacement extremums. The flipping factor of the voltage bias-flip action is denoted as γ.[19]

The conceptual development toward the dual-effect broadband solution is illustrated by the frequency responses of four systems in Fig. 2. The −3 dB (half-maximum-power) bandwidth is used to evaluate the broadband capability of different energy harvesting solutions.[21] From Figs. 2(a) and 2(b), it is found that the vibration bandwidth has been broadened by many folds because of the introduction of nonlinearity (NL) to a linear PEH (L-PEH) device, both under the open-circuit condition. However, when connected with an ac-to-dc interface circuit for rectification, such as the SS interface circuits, which is of necessity toward practical use of the harvested energy, the orbit hysteresis in the nonlinear structure shrinks significantly. As a result, the bandwidth-broadening effect contributed by mechanical nonlinearity is impaired due to the increase in electrically induced damping in a practical PEH system, as shown in Fig. 2(c). The purpose of introducing PVSS from the electrical side is to compensate such bandwidth shrinking since the PVSS control has been proven as an electrical bandwidth-broadening solution in the literature.[17–19] The idea from NL-SS-PEH to NL-PVSS-PEH is illustrated by the progression from Figs. 2(c) and 2(d). As shown by the blue and red trajectories, either phase-lead ($\varphi < 0$) or phase-lag ($\varphi > 0$) case increases the hysteresis, which results in a rebound of the bandwidth broadening effect.

Under harmonic base excitation, whose acceleration is $\ddot{y}(t)$, the dynamics of an NL-PVSS-PEH system can be approximated by a lumped-parameter model, whose schematic is shown in Fig. 3. The dynamic model can be broken down into three parts: a linear vibrator composed of the equivalent mass M, damping D, and stiffness K, which represents the main cantilevered beam; additional stiffnesses including linear K_1 and nonlinear K_2, which are introduced by the two repelling magnets;[7] and the electrically induced dynamic components including a tunable stiffness/mass K_e and a tunable damping D_e, which are produced by the PVSS controlled interface circuit through electrical-to-mechanical coupling.[19] The equivalent mechanical representation can also be converted into an equivalent electrical impedance network through electromechanical analogy,[22] which is not repeated here. The dynamic relation can be mathematically expressed by a constitutive equation as follows:

$$M\ddot{x} + (D + D_e)\dot{x} + \left(K + K_1 + K_2x^2 + K_e\right)x = -M\ddot{y}. \quad (1)$$

Equation (1) is inclusive. It can describe any of the four systems in Fig. 2 by selecting different parameters in the NL and PVSS blocks.

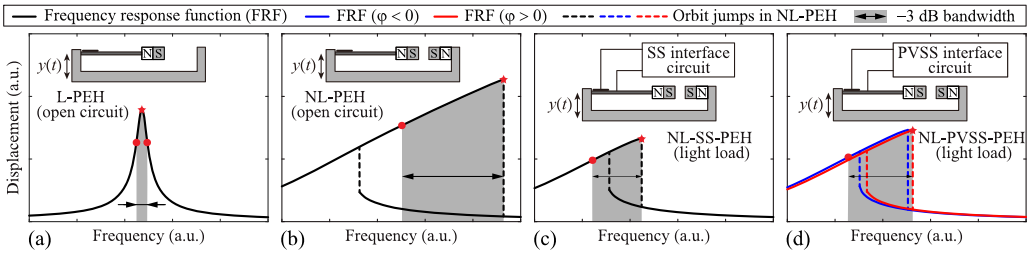

FIG. 2. Conceptual development from linear PEH to nonlinear PVSS PEH systems. Sub-figures show the schematics and frequency responses of (a) linear PEH system, (b) nonlinear PEH system, (c) nonlinear PEH system using the SS circuit, and (d) nonlinear PEH system using the PVSS circuit.

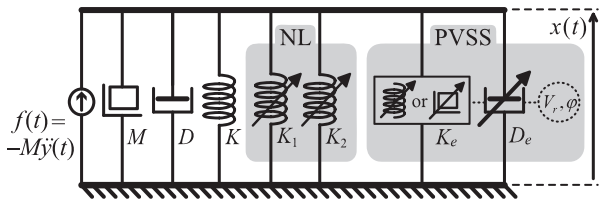

FIG. 3. Equivalent lumped-parameter model of a dual-effect NL-PVSS-PEH system.

TABLE I. Parameters of the monostable piezoelectric system.

Parameter	Value	Parameter	Value
M	8.61 g	α	0.127 mN/V
D	0.011 Ns/m	A_Y	1 m/s^2
K	51.50 N/m	C_p	35.61 nF
K_1	−41.45 N/m	R_p	713 kΩ
K_2	226.70 kN/m^3	γ	−0.2

K_1 and K_2 are adjustable by tuning the magnet gap, while K_e and D_e are electrically tunable by changing the rectified voltage V_r and switching phase difference φ in the PVSS controlled interface circuit.[19]

In the PVSS controlled interface circuits, the electrically induced damping D_e and stiffness/mass K_e can be quantified based on the equivalent impedance analysis in the electrical domain.[22] Taking PV-S3BF, whose circuit topology is shown in Fig. 1, as an example, the mechanically induced current i_{eq} as well as the piezoelectric voltage v_p and its fundamental harmonic $v_{p,f}$ are shown in Figs. 4(a)–4(c) for phase-lead, in-phase, and phase-lag cases, respectively. Their corresponding electrically induced impedance is marked by solid dots in Fig. 4(d). In the equivalent impedance analysis, the circuit dynamics can be linearly approximated according to the magnitude and phase relations between $v_{p,f}$ and i_{eq}, in terms of electrical impedance, i.e.,

$$Z_e(\omega, V_r, \varphi) = \frac{V_{p,f}(j\omega)}{I_{eq}(j\omega)} = R_e(\omega, V_r, \varphi) + jX_e(\omega, V_r, \varphi), \quad (2)$$

where $V_{p,f}$ and I_{eq} are the frequency-domain expressions of $v_{p,f}$ and i_{eq}; ω is the operating frequency. The Z_e expression differs with different circuit solutions. It also depends on piezoelectric capacitance C_p, dielectric leakage resistance R_p, and flipping factor γ. Equation (2) just shows the key step in the electrical dynamics modeling. Detailed Z_e formulas of different interface circuits were elaborated in the literature.[19,22–24]

The electrically induced damping D_e and stiffness/mass K_e can be derived based on the electromechanical analogy in this coupling system, i.e.,

$$D_e = \alpha^2 R_e, \quad K_e = -\alpha^2 \omega X_e, \quad (3)$$

where α is the force-to-voltage coupling factor. The two additional components generalized the equivalent dynamics produced by the interface circuit through electromechanical coupling; therefore, they are called electrically induced dynamic components. When the system operates at a specific frequency ω, the electrically induced D_e and K_e are functions of V_r and φ, whose picture can be mapped on a two-dimensional D_e-K_e plane. With one set of parameters extracted from the experimental setup, as shown in Table I, the available range of the D_e-K_e pair with different interface circuits under 8 Hz vibration is shown in Fig. 4(d).

The covered area by different PVSS control circuits is in circular shapes.[19] Compared to PV-SCE and PV-SSHI, the PV-S3BF solution allows the largest horizontal span, which corresponds to the electrically induced damping component D_e. With the PVSS control, varying the switch phase φ enlarges the vertical span of the area, which

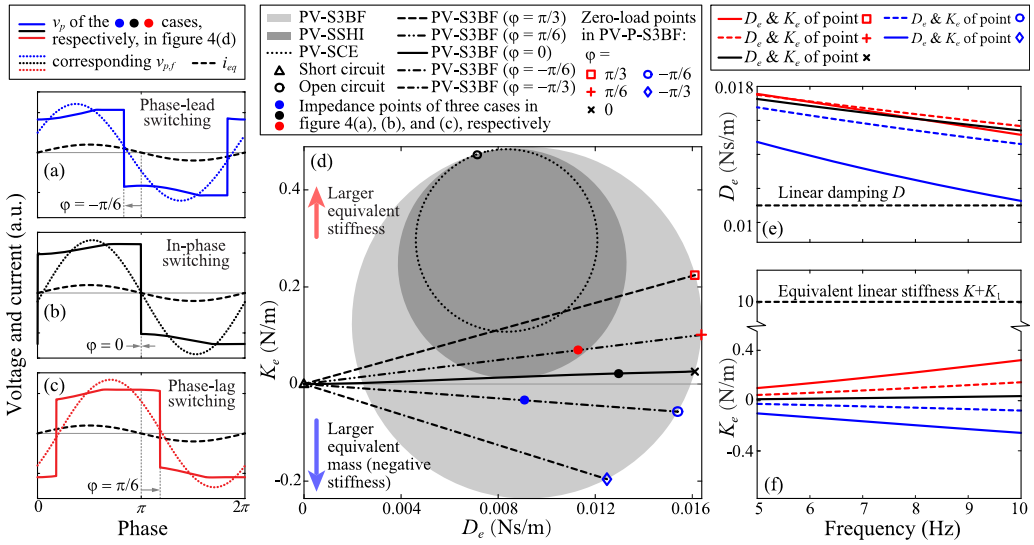

FIG. 4. Features of the PV-S3BF interface circuit. (a)–(c) Operating voltage and current waveforms under different switch phase lead/lag. (d) Equivalent impedance ranges of different circuits at 8 Hz vibration. (e) and (f) Electrically induced damping D_e and stiffness/mass K_e under the zero-loading condition.

corresponds to the electrically induced stiffness K_e (the dynamics of a negative K_e is equivalent to the effect of a mass). Therefore, it can enhance the energy harvesting capability and, meanwhile, broaden the bandwidth. The D_e and K_e values of some extreme magnitude points (light-load condition) with different switch phases ($\varphi = -\pi/3, -\pi/6$, 0, $\pi/6$, and $\pi/3$) are illustrated in Figs. 4(e) and 4(f). The damping coefficient D and stiffness K of the linear vibrator are also shown in the figures for comparison. It shows that the electrically induced damping is comparable to the mechanical damping, which means that the circuit can attain the impedance matching point under resonance. On the other hand, the magnitude of the electrically induced stiffness/mass is much smaller than the mechanical stiffness. It shows that the dynamic tunability ranges from about $0.2/10 = 2\%$ at 5 Hz to $0.6/10 = 6\%$ at 10 Hz when φ in PVSS varies in between $-\pi/3$ and $\pi/3$.

In general, by tuning a PEH interface circuit with PVSS control, the frequency response of a vibrator, no matter linear or nonlinear, using such an interface circuit can be adjusted to some extent. A dual-effect broadband PEH system can be realized by organically incorporating a nonlinear structure on the mechanical side and PVSS control on the electrical side.

To theoretically figure out the vibration magnitude X, we use the harmonic balance method[7] to solve the equation of motion in (1). Assuming that the displacement X is periodic and can be approximated by its fundamental harmonic, by substituting the displacement assumption into Eq. (1), and balancing the first-order harmonics, a nonlinear algebra equation can be derived as follows:

$$\left[\left(K + K_1 + K_e + \frac{3K_2X^2}{4} - M\omega^2\right)^2 + \omega^2(D + D_e)^2\right]X^2 = M^2A_Y^2, \tag{4}$$

where $A_Y = \omega^2 Y$ is the base acceleration magnitude (Y is the base displacement magnitude). The theoretical value of X under different conditions is obtained by numerically solving transcendental Eq. (4).

Experiments are carried out to validate the theoretical analysis of the dual-effect broadband PEH system. The main structure of the experimental setup is a monostable piezoelectric cantilevered beam whose parameters are shown in Table I. A PV-S3BF circuit is connected and tuned for adjusting the dynamics on the electrical side. A laser vibrometer (OFV-552/5000, Polytec) is used to measure the vibration velocity and displacement. Given that the piezoelectric equivalent current source i_{eq} is proportional to vibration velocity, the output velocity signal is also used to provide synchronization for switch control. The switch control is executed by a microcontroller (MSP430F2274, Texas Instrument) and eight MOSFET switches. The theoretical and experimental displacements in NL-PEH, NL-SS-PEH ($\varphi = 0$), and NL-PVSS-PEH (φ is not confined) are comparatively shown in Fig. 5. The experimental results show a good agreement with the theoretical analysis. By taking the effective bandwidth broadening mechanisms on both the mechanical and electrical sides, a more advanced dual-effect broadband solution is realized in a practical PEH system. The −3 dB bandwidths of NL-SS-PEH and NL-PVSS-PEH are shown in Fig. 5(b) by the gray area and the light gray area, respectively. Compared to NL-SS-PEH, after taking the PVSS control, the −3 dB bandwidth of NL-PVSS-PEH has been improved by 18.7%

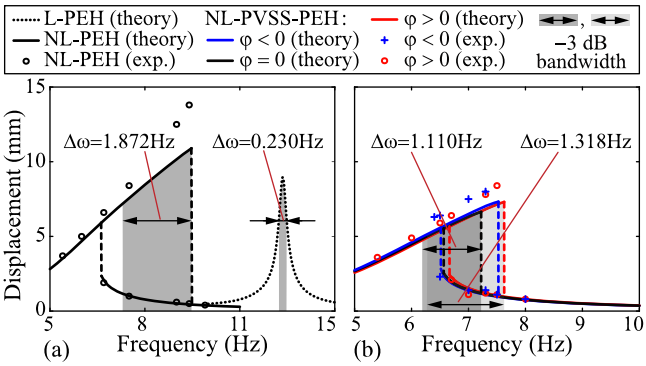

FIG. 5. Theoretical and experimental results. (a) L-PEH and NL-PEH. (b) NL-PVSS-PEH.

[$\Delta\omega$ from 1.110 Hz to 1.318 Hz, as shown in Fig. 5(b)] in the experiment.

In summary, this Letter has introduced a dual-effect solution toward broadband PEH design. The first broadband effect was introduced on the mechanical side by introducing mechanical nonlinearity into a linear PEH system. Mechanical nonlinearity brings out the additional stiffness K_1 and K_2 to the system and produces orbit hysteresis. The second broadband effect was realized on the electrical side by utilizing the PVSS control in PEH interface circuits. PVSS control not only induces an extra damping effect D_e to the PEH system, as the SS control does, but also produces an extra stiffness/mass K_e to the system. In particular, the electrically induced K_e realizes the off resonance compensation to some extent, so as to contribute to the bandwidth broadening capability in an electrical way. The dual-effect NL-PVSS-PEH offers a design perspective to implement the PVSS control into nonlinear energy harvesting systems and provides an integrated solution toward practical broadband and high-capability vibration energy harvesting systems.

The work described in this paper was supported by the National Natural Science Foundation of China (Project No. 61401277) and the Research Grants Council of Hong Kong Special Administrative Region, China (Project No. CUHK 14205917).

REFERENCES

[1]F. K. Shaikh and S. Zeadally, Renewable Sustainable Energy Rev. **55**, 1041 (2016).
[2]L. Xiong, L. Tang, and B. R. Mace, Appl. Phys. Lett. **108**, 203901 (2016).
[3]S. Zhou, J. Cao, D. J. Inman, S. Liu, W. Wang, and J. Lin, Appl. Phys. Lett. **106**, 093901 (2015).
[4]T. Huguet, A. Badel, and M. Lallart, Appl. Phys. Lett. **111**, 173905 (2017).
[5]J. Wang, S. Zhou, Z. Zhang, and D. Yurchenko, Energy Convers. Manage. **181**, 645 (2019).
[6]K. Fan, M. Cai, F. Wang, L. Tang, J. Liang, Y. Wu, H. Qu, and Q. Tan, Energy Convers. Manage. **198**, 111820 (2019).
[7]S. C. Stanton, B. A. M. Owens, and B. P. Mann, J. Sound Vib. **331**, 3617 (2012).
[8]R. L. Harne and K. Wang, Smart Mater. Struct. **22**, 023001 (2013).
[9]M. F. Daqaq, R. Masana, A. Erturk, and D. Dane Quinn, Appl. Mech. Rev. **66**, 040801 (2014).
[10]P. Firoozy, S. E. Khadem, and S. M. Pourkiaee, Int. J. Eng. Sci. **111**, 113 (2017).
[11]I. Ayala-Garcia, P. Mitcheson, E. Yeatman, D. Zhu, J. Tudor, and S. Beeby, Sens. Actuators, A **189**, 266 (2013).

[12]S.-K. Lai, C. Wang, and L.-H. Zhang, Mech. Syst. Sig. Process. **122**, 87 (2019).
[13]Y. C. Shu, I. C. Lien, and W. J. Wu, Smart Mater. Struct. **16**, 2253 (2007).
[14]D. Guyomar, A. Badel, E. Lefeuvre, and C. Richard, IEEE Trans. Ultrason., Ferroelectr., Freq. Control **52**, 584 (2005).
[15]J. Liang, Y. Zhao, and K. Zhao, IEEE Trans. Power Electron. **34**, 275 (2019).
[16]J. R. Liang and W. H. Liao, J. Intell. Mater. Syst. Struct. **20**, 515 (2009).
[17]E. Lefeuvre, A. Badel, A. Brenes, S. Seok, and C.-S. Yoo, J. Intell. Mater. Syst. Struct. **28**, 2988 (2017).
[18]P.-H. Hsieh, C.-H. Chen, and H.-C. Chen, IEEE Trans. Power Electron. **30**, 3142 (2015).
[19]B. Zhao, J. Liang, and K. Zhao, in *IEEE International Symposium on Circuits and Systems* (IEEE, 2018), pp. 1–5.
[20]A. Morel, G. Pillonnet, P. Gasnier, E. Lefeuvre, and A. Badel, Smart Mater. Struct. **28**, 025009 (2019).
[21]A. Cammarano, S. Neild, S. Burrow, and D. Inman, Smart Mater. Struct. **23**, 055019 (2014).
[22]J. Liang and W. Liao, IEEE/ASME Trans. Mechatron. **17**, 1145 (2012).
[23]J. Liang, H. S. H. Chung, and W. H. Liao, Smart Mater. Struct. **23**, 092001 (2014).
[24]J. Wang, B. Zhao, J. Liang, and W.-H. Liao, Smart Mater. Struct. (in press).